Proceedings of the Seventh International Conference on
Railway Technology: Research, Development and Maintenance
Edited by: J. Pombo
Civil-Comp Conferences, Volume 15, Paper 3.8
Civil-Comp Press, Edinburgh, United Kingdom, 2026
ISSN: 2753-3239, doi: 10.4203/ccc.15.3.8


# Machine Learning-Based Estimation of Wheel-Rail Contact Conditions from Instrumented Wheelset Data

**K. Nakano[1], K. Yabuuchi[1], S. Kuniyuki[2], W. Wang[1], K. Iida[2], T. Tanaka[2] and T. Miyamoto[3]**

**[1]Institute of Industrial Science, The University of Tokyo, Japan**
**[2]Railway Technical Research Institute, Japan**
**[3]Meisei University, Japan**

## Abstract

This study proposes a machine learning-based method to estimate wheel–rail contact conditions from instrumented wheelset (PQ wheelset) measurements for running safety assessment. A multibody dynamics-based vehicle dynamics simulation is used to generate large training datasets covering various speeds, curve radii, and friction conditions. LightGBM and a one-dimensional convolutional neural network are adopted to estimate the angle of attack, lateral contact position, and friction coefficient. Validation under unseen loading and track irregularity conditions demonstrates sufficient practical estimation accuracy over a wide range of speeds and curve radii, supporting real-time safety evaluation.

**Keywords:** running safety assessment, instrumented wheelset, wheel–rail contact conditions, angle of attack, friction coefficient, machine learning.

## 1 Introduction

Derailment is one of the factors that compromise the running safety of railways, and among its various forms, the prevention of flange-climb derailment, in which a wheel climbs onto the rail, is of particular importance. For the assessment of running safety, the ratio of the lateral force $Y$ or $L$ to the vertical wheel load $Q$ or $V$ known as the derailment coefficient $Y/Q$ or $L/V$ is commonly used. In Japan, $Q$ is conventionally used in place of $Y$ and $L$, and $P$ is used in place of $Q$ and $V$ (this paper will also use $Q$ and $P$ hereafter). In practice, running tests are conducted using an instrumented wheelset (PQ wheelset) equipped with strain gauges, as shown in Figure 1, and safety is evaluated by comparing the measured values with the critical derailment coefficient derived from Nadal's formula.

There are currently two main challenges in safety assessment. First, the critical derailment coefficient includes uncertain parameters, such as the friction coefficient, which vary depending on operating conditions. As a result, current evaluations rely on comparisons with reference values that incorporate safety margins, and there is a need to accurately capture the actual wheel–rail contact conditions. To address this issue, a physics-based approach using state estimators such as the Kalman filter was proposed[1]; however, challenges remain regarding the complexity of parameter tuning and the computational burden for real-time implementation. Second, the analysis of PQ measurement data depends heavily on expert knowledge, leading to issues of subjective interpretation of causal factors and difficulties in knowledge transfer. To address these challenges, this study proposes a machine learning-based method for estimating wheel–rail contact conditions that influence PQ measurement data, enabling objective decision support with real-time capability. By visualizing the underlying track displacement embedded in PQ measurement data, together with the estimation of wheel–rail contact conditions, this study aims to enhance and automate the evaluation of railway running safety.

Figure 1: Overview of the Instrumented wheelset.

## 2 Methods

### 2.1 Vehicle dynamics simulation model

In order to obtain a large amount of PQ measurement data required for machine learning, along with the corresponding ground truth of contact conditions and track displacement, the authors first generate a large-scale dataset based on a physics-based simulation model. This dataset is then used as training data to construct the machine learning model. Next, the validity of the developed model is evaluated using validation data obtained from simulations. A standard bogie vehicle operating on Japan's narrow-gauge railway lines was assumed, and a single-vehicle model was constructed based on its specifications. The wheel profile was defined using the design shape of a modified arc tread, while the rail profile was modelled based on the design geometry of the JIS 50kgN rail. The creep forces between the wheel and rail were calculated using FASTSIM, a simplified theory proposed by Kalker[2]. As track conditions, in the constant curve section, the cant $C$ was set to 105 mm and the slack $S$ to 0 mm, both treated as constant values. In the transition curve, both the cant and curvature vary proportionally with the distance from the beginning of the transition. Unless otherwise specified, the friction coefficient was set to 0.4. As analysis parameters, a dataset was generated by widely varying the running speed $V$, curve radius $R$, and the wheel–rail friction coefficient $\mu$.

The track displacement was generated using a power spectral density (PSD) approach. The PSD functions employed were those proposed by the Federal Railroad Administration (FRA) in the United States and by German standards[3][4]. When using the German formulation, the parameters were adjusted so that the generated track displacement corresponded to each FRA class. Specifically, taking advantage of the fact that the integral of the PSD corresponds to the variance of the displacement (i.e., the square of the standard deviation), the roughness coefficient in the generation formula was determined such that the integrated PSD values of the two formulations became equivalent.

### 2.2 Machine learning model

LightGBM[5] and a one-dimensional convolutional neural network (1D-CNN)[6] were adopted as the machine learning algorithms. Specifically, LightGBM was used to estimate the wheel–rail contact conditions, namely, the angle of attack and the left/right contact positions, while the 1D-CNN was employed to estimate the friction coefficient in the contact conditions. The former was selected because of its ability to capture nonlinear relationships with high accuracy and computational efficiency. The latter was adopted because it is well suited for extracting physical quantities, such as the friction coefficient, from time-series data like PQ measurements, owing to its strength in modelling temporal dependencies.

As explanatory variables, the time-series signals obtained from PQ measurements using an instrumented wheelset were primarily used, including the vertical wheel load $P$, lateral force $Q$, and longitudinal tangential force $T$ for both the left and right wheels. In addition to these, the contact phase difference between the left and right wheels, as well as the track curvature and running speed representing track and operating conditions, were adopted as parameters. The contact phase is defined as the longitudinal displacement of the contact point relative to the lowest point of the wheel, expressed in terms of an angle, and the difference between the left and right wheels is referred to as the contact phase difference. For these basic variables, feature engineering was performed in accordance with the input format of the estimation methods, including the computation of statistical and physical quantities and the segmentation of time-series data using a sliding window, thereby constructing a feature set effective for estimation.

The target variables were defined as physical quantities directly related to the evaluation of vehicle running safety and the assessment of track conditions. Specifically, three quantities representing the wheel–rail contact state were selected: the angle of attack, the left/right contact positions, and the friction coefficient. The angle of attack is defined as the relative yaw angle between the rail and the wheelset.

The left/right contact positions refer to the lateral locations of the contact points (i.e., the centres of the contact patches) between the wheel and rail on the wheel tread. The friction coefficient is a parameter that determines the limiting value of the tangential force at the wheel–rail contact interface. It is a key factor in determining the critical derailment coefficient (Nadal's criterion), and its accurate estimation is therefore essential.
To address the black-box nature of the machine learning model and to clarify the mechanical basis underlying its estimations, feature importance in LightGBM and SHAP (SHapley Additive exPlanations) were employed. These methods enable the visualization of how each feature contributes to the estimation results.

## 3 Simulation

Based on the characteristics of the target variables, the training datasets were constructed by classifying them into two types: one for the estimation of the angle of attack and lateral contact position, and the other for the estimation of the friction coefficient. The running speed $V$ was set from 10 km/h to 100 km/h in increments of 10 km/h, resulting in 10 conditions. The curve radius $R$ was set from 200 m to 1000 m in increments of 100 m, resulting in 9 conditions. For the dataset used to estimate the angle of attack and contact position, running data on an S-shaped track were adopted, where the vehicle enters a right curve after passing through a straight section following a left curve. This configuration aims to comprehensively capture transient changes in contact conditions during curve entry and exit, as well as in reverse curves. Figure 2 shows the curvature profile of the track used. For the dataset used to estimate the friction coefficient, only data from left-curve running were used to improve the learning efficiency of the estimation model. In this dataset, a wide range of contact conditions was considered by varying the friction coefficient $\mu$ from 0.1 to 0.8 in increments of 0.1, representing conditions from dry to wet. Figure 3 shows the corresponding curvature profile of the track.

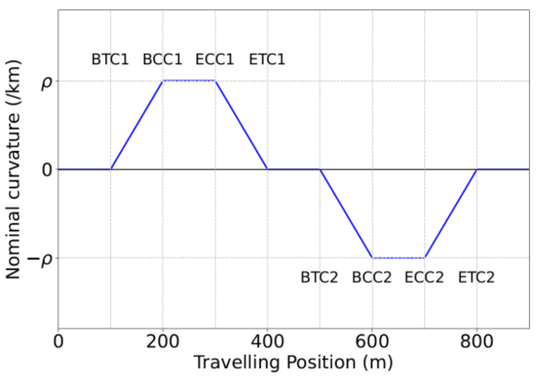


Figure 2: Nominal curvature for wheel angle of attack and lateral contact position.

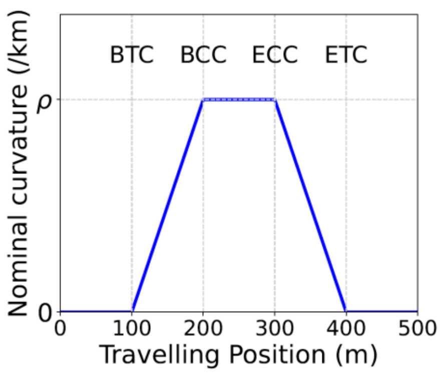


Figure 3: Nominal curvature for friction coefficient.

To evaluate the generalization performance of the constructed estimation models and their accuracy under unseen running conditions, a validation dataset was developed using conditions not included in the training data. Specifically, the curve radius $R$ was varied from 250 m to 1050 m in increments of 100 m, resulting in 9 conditions. For the validation dataset used for friction coefficient estimation, the friction coefficient $\mu$ was varied from 0.05 to 0.75 in increments of 0.1, resulting in 8 conditions.

In addition, two conditions were modified from those used in the training data. First, the vehicle loading condition was changed from an empty vehicle to a fully loaded condition with 200 passengers. Second, track irregularities were superimposed. Based on the above conditions, two patterns were defined as shown in Table 1. The curvature profile of the test track is same as that shown in Figure 3. The same explanatory variables were used for all target variables, namely the angle of attack, the left and right contact positions, and the friction coefficient. Specifically, the wheel load $P$, lateral force $Q$, and longitudinal creep force $T$of both left and right wheels were used. Furthermore, derived mechanical indicators were included: the derailment coefficient $Q/P$ and the tangential force coefficient $\mu T/P$. In addition, the phase difference in contact between the left and right wheels, $\Delta\phi$, was introduced. Moreover, to account for vehicle running conditions and track geometry, the running speed $V$ and curvature $1/R$ were adopted as input features.

| **Pattern** | **Training** | | **Validation** | |
|---|---|---|---|---|
| | Load | Irregularity | Load | Irregularity |
| | Unloaded | None | Loaded* | None |
| | Unloaded | FRA ** | Unloaded | German** |

Table 1. Experimental conditions for training and validation datasets, where *Loaded: Payload of 200 passengers (11 t) added, **FRA/German: Track irregularity PSD models.

# 4 Results

## 4.1 Angle of attack

Estimation was performed for each trial (i.e., each combination of curve radius and running speed) in the validation datasets for Pattern 1 and Pattern 2, and quantitative evaluation was conducted using the root mean square error (RMSE). The overall trends in estimation accuracy across all trials are presented as heatmaps. Feature importance is shown for the top seven features.

Figure 4 (a) shows the RMSE distribution as a heatmap for each combination of running speed and curve radius. As observed in the figure, Pattern 1 maintains consistently low RMSE values regardless of variations in speed and radius, indicating that the proposed model exhibits strong robustness to changes in vehicle mass. A more detailed analysis of the error trends reveals that, when the running speed is fixed, RMSE tends to increase as the curve radius decreases, with particularly pronounced errors in tight curves with radii of 250 m and 350 m. On the other hand, when focusing on speed dependency under a fixed curve radius, larger-radius curves (greater than

650 m) exhibit higher errors at lower speeds. In contrast, for small-radius curves, RMSE attains its minimum within the speed range of 30 km/h to 70 km/h, and increases as the speed deviates from this range in either direction.

Figure 4 (b) shows the RMSE distribution as a heatmap for each combination of running speed and curve radius. Compared with Pattern 1, which assumes ideal track conditions, Pattern 2 exhibits an overall increase in RMSE due to the influence of track irregularities generated using the German PSD formulation as disturbances in the validation data.

Nevertheless, severe degradation in estimation accuracy is avoided across all trials, confirming that the proposed method maintains high generalization performance even under conditions where track irregularities are introduced using a different PSD model (German formulation) from that used during training (FRA formulation). Regarding error trends, in contrast to Pattern 1, where larger errors were observed in low-speed and small-radius conditions, Pattern 2 shows a clear tendency for RMSE to increase with increasing running speed. Additionally, under fixed-speed conditions, RMSE tends to increase as the curve radius becomes larger.

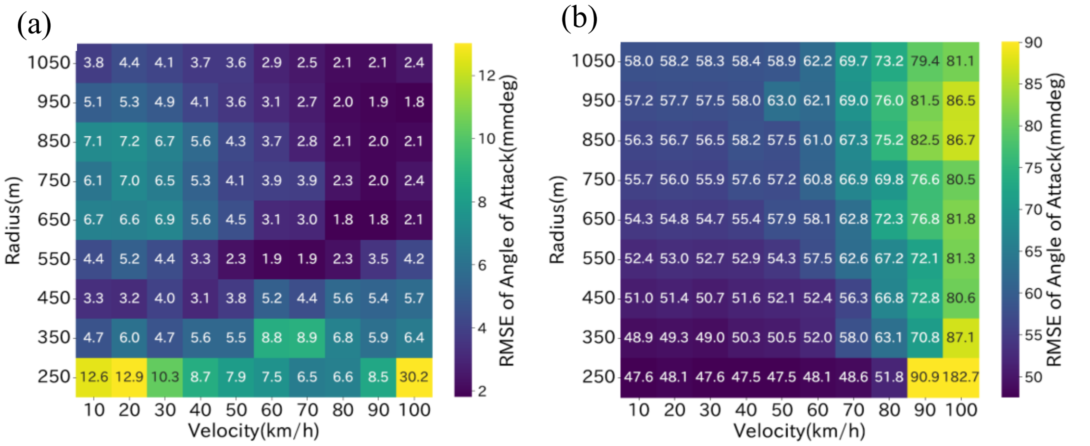


Figure 4: Heatmaps of RMSE for wheel angle of attack estimation across various speeds and curve radii, where (a) and (b) represent the results of Pattern 1 and 2, respectively.

To examine which physical quantities the proposed model focuses on in performing the estimation, the feature importance for angle-of-attack estimation is shown in Figure 5 (a). Note that the suffixes "in" and "out" in the feature names represent the inner-rail and outer-rail sides, respectively. As shown in the figure, the estimation model depends most strongly on the contact phase difference $\Delta\theta$, followed by the curvature, which is the inverse of the curve radius. This is consistent with the proportional relationship between the angle of attack $\psi_\omega$ and the contact phase difference $\Delta\phi$.

Furthermore, it is known that the geometrically determined angle of attack, $G\psi_\omega$, is proportional to the curvature $(1/R)$[7], suggesting that the model has learned relationships grounded in physical principles. The corresponding relationships are given as

$$G\psi_{\omega} \approx \frac{2\omega}{R} \tag{1}$$

$$\Delta\theta \approx \psi_{\omega}(\tan\alpha_2 - \tan\alpha_1) \tag{2}$$

Here, $\alpha_1$and $\alpha_2$denote the contact angles between the wheel and rail, $2\omega$ represents the wheelbase, and $R$ is the curve radius. In the time-series data, a steady-state error was observed in the curved sections. This is considered to be due to the influence of the change in vehicle load on the contact phase difference, which altered its response in the curved sections. As a result, the estimated angle of attack was also affected, leading to a steady offset in the estimation results.

In Pattern 2, the physical factors contributing to the increase in RMSE under different running conditions are discussed. Focusing on the effect of curve radius, it was observed that, under the same speed conditions, the amplitude of variation in the angle of attack tends to increase as the curve radius becomes larger. In such regions with larger amplitudes, the model tends to output underestimated values, which likely leads to larger errors for larger-radius curves.

Furthermore, the feature importance for angle-of-attack estimation in Pattern 2 is shown in Figure 5 (b). Compared with Pattern 1, the model exhibits an excessively high dependence on the contact phase difference, while the correlation with curvature is reduced. This suggests that, due to the addition of track irregularities, the unique geometric relationship between the angle of attack and curvature is no longer preserved. As a result, the model is unable to effectively utilize curvature information and instead relies excessively on the contact phase difference, which reflects the instantaneous wheel–rail contact state. Consequently, this shift in dependency is considered to be one of the reasons why Pattern 2 exhibits larger estimation errors than Pattern 1.

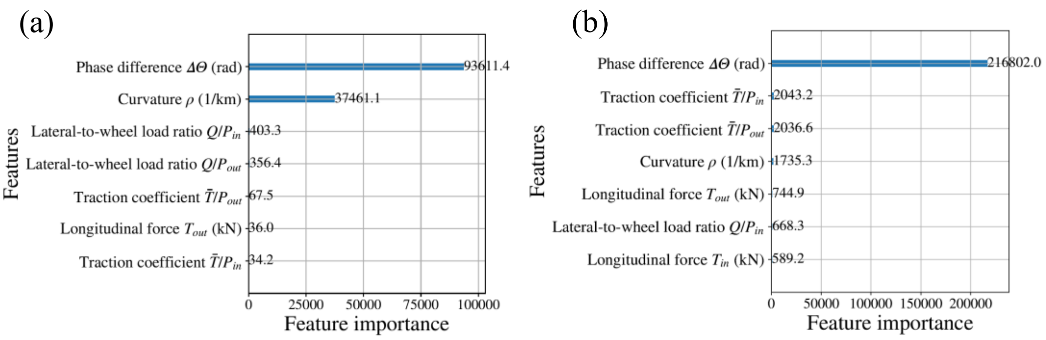


Figure 5: Feature importance for the wheel angle of attack estimation model, where (a) and (b) are results of Pattern 1 and 2, respectively.

## 4.2 Contact position on the outer rail

Estimation was performed for each trial (i.e., each combination of curve radius and running speed) in the validation datasets for Pattern 1 and Pattern 2, and quantitative evaluation was conducted using RMSE. The overall trends in estimation accuracy across all trials are presented as heatmaps. Figure 6 (a) shows the RMSE distribution as a heatmap for each combination of running speed and curve radius. Similar to the angle of attack, Pattern 1 demonstrates that the proposed model maintains high robustness to variations in vehicle mass regardless of changes in speed and curve radius. In addition, a tendency for increased RMSE is observed under conditions of low running speed and large curve radius. Figure 6 (b) shows the RMSE distribution as a heatmap for each combination of running speed and curve radius. Analysis of the error trends reveals that, under fixed-speed conditions, RMSE tends to increase as the curve radius increases. Furthermore, when the curve radius is fixed, the estimation accuracy deteriorates with increasing running speed.

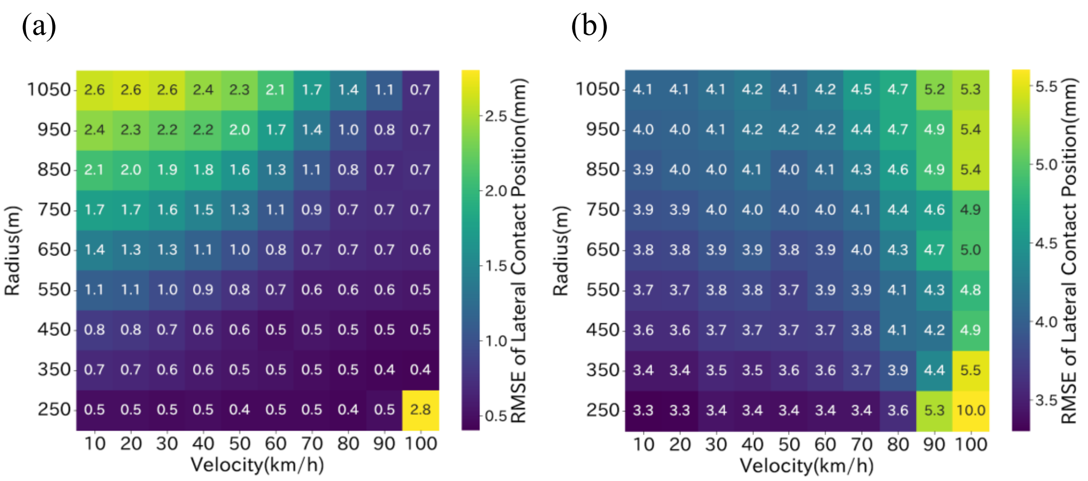


Figure 6: Heatmaps of RMSE for lateral contact position estimation across various speeds and curve radii, where (a) and (b) represent the results of Pattern 1 and 2, respectively.

It can be observed that the estimation accuracy on the outer rail side deteriorates under conditions of large-radius curves and low-speed running (upper-left region of the heatmap). This is likely because, under such conditions, the force pressing the wheelset toward the outer rail is insufficient during curve negotiation, and consequently, variations in the contact position are not clearly reflected as mechanical responses in the PQ measurement data. In addition, the change in vehicle load in the validation data (empty versus fully loaded conditions) is considered to have caused deviations in creep characteristics and force balance within the contact patch from those assumed during training, which also contributed to the degradation in estimation accuracy.

Based on the feature importance in Pattern 1, as shown in Figure 7 (a), the estimation method of the model is analyzed. For the outer rail side, curvature exhibits the highest contribution, indicating that the geometric conditions of the track play a dominant role in determining the steady-state contact position. This suggests that, under ideal track conditions, the contact position, similar to the angle of attack, strongly depends on geometric relationships governed by curvature. From these results, it can be inferred that the proposed model maintains high estimation performance against variations in

vehicle load by effectively leveraging the relationship between track geometry and bogie dynamics.
The feature importance for contact position estimation in Pattern 2 is shown in Figure 7 (b). Compared with Pattern 1, the importance of curvature, a geometric physical quantity, is reduced. This is because the addition of track irregularities disrupts the unique geometric relationship between curvature and contact position. Furthermore, the tangential force coefficient serves as an indicator that indirectly reflects the steering moment state of the bogie. Notably, the tangential force coefficient of the wheel on the opposite side of the estimation target shows the highest importance. This suggests that the proposed model estimates the contact position under disturbed conditions by extracting features not only from the local mechanical response of the target wheel but also from the overall steering balance of the bogie, including the opposing wheel.

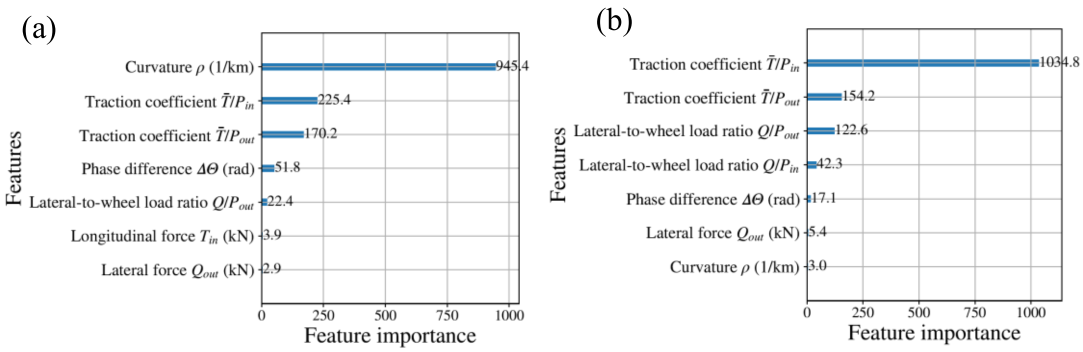


Figure 7: Feature importance for the lateral contact position estimation model, where (a) and (b) represent the results of Pattern 1 and 2, respectively.

### 4.3 Friction coefficients

Estimation was performed for each trial (i.e., each combination of curve radius and running speed) in the validation datasets for Pattern 1 and Pattern 2, and quantitative evaluation was conducted using RMSE. The overall trends in estimation accuracy across all trials are presented as heatmaps. Figure 8 (a) shows the heatmap of RMSE distribution for each combination of running speed and curve radius. In this analysis, RMSE was calculated using data extracted from the 100 m to 400 m section, which includes both transition curves and circular curves where friction coefficient estimation was performed with high accuracy.
Under fixed curve radius conditions, RMSE increases with increasing running speed. Similarly, under fixed-speed conditions, RMSE increases with increasing curve radius. Analysis of the time-series data indicates that, under low-speed and low-friction conditions, high tracking performance with respect to the ground truth is achieved not only in circular curves but also in transition curve sections. In contrast, under high-friction conditions, the duration over which the estimates can follow the ground truth becomes shorter. Furthermore, estimation was not feasible in straight sections under any speed condition.

Figure 8 (b) shows the heatmap of RMSE distribution for each combination of running speed and curve radius. In contrast to the results of Pattern 1 and Pattern 2, with added track irregularities, shows an overall improvement in estimation accuracy.
A detailed analysis of the error trends reveals that, under fixed curve radius conditions, RMSE deteriorates with increasing running speed. On the other hand, the influence of curve radius on RMSE becomes relatively smaller. Moreover, the time-series results indicate that, unlike Pattern 1, estimation becomes feasible even in straight sections.

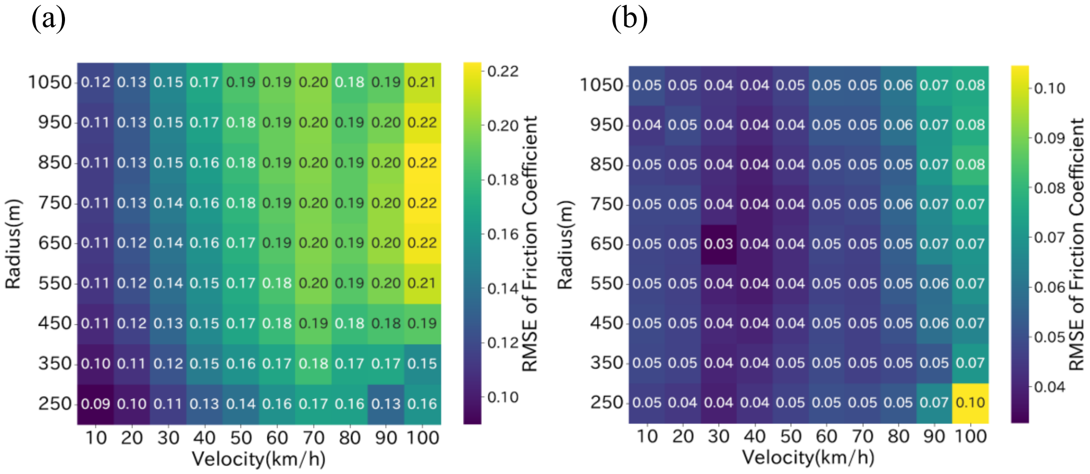


Figure 8: Heatmaps of RMSE for friction coefficient estimation across various speeds and curve radii, where (a) and (b) represent the results of Pattern 1 and 2, respectively.

From the obtained time-series data, the proposed method tends to exhibit better estimation performance in transition and circular curve sections compared with straight sections. This is likely because slip between the wheel and rail is more likely to occur in curved sections, and as the slip ratio increases, the creep force approaches saturation near the friction limit. As a result, it becomes physically easier to inversely estimate the friction coefficient from the mechanical response.
Figure 9 (a) shows the SHAP values (mean absolute values) of the top seven features. It can be observed that the lateral-to-vertical force ratio ($Q/P$) and the running speed are among the top three most important features. In particular, the fact that the lateral-to-vertical force ratio on the inner rail side is identified as the most important feature is consistent with the physical property that, under conditions where creep forces are saturated, such as in sharp curves, the inner-side $Q/P$ can be regarded as approximately equivalent to the friction coefficient. Furthermore, the high importance of running speed suggests that the model has learned to account for speed-dependent effects.
The estimation accuracy and error factors of the friction coefficient in Pattern 2 are discussed. Similar to Pattern 1, the estimation error increases with increasing running speed. This is considered to be due to the fact that, as speed increases, the influence of dynamic vibrations induced by track irregularities becomes more pronounced, thereby intensifying disturbances in the PQ measurement data used as input signals.
An examination of the time-series data reveals that, even in trials with relatively low overall accuracy, the estimated values tend to approach the ground truth in transition

and circular curve sections. This is because, in straight sections where steady slip does not occur, information on the friction coefficient is not sufficiently reflected in the force data, whereas in curved sections, slip occurs and provides the necessary physical information for estimation.
On the other hand, unlike the results of Pattern 1, Pattern 2 shows relatively good estimation performance even in straight sections. This is likely because the addition of track irregularities creates conditions in which slip between the wheel and rail is more likely to occur even in straight sections. In other words, the track irregularities, acting as disturbances, may contribute to extracting friction-related characteristics. The SHAP analysis results shown in Figure 9 (b) indicate that, although the overall trend is similar to that of Pattern 1, the contribution of features beyond the top three increases in Pattern 2. In particular, the importance of the longitudinal creep force becomes higher. This suggests that, due to the increased complexity of the force response caused by track irregularities, the model utilizes a broader combination of features, including longitudinal creep force, to estimate the friction coefficient.

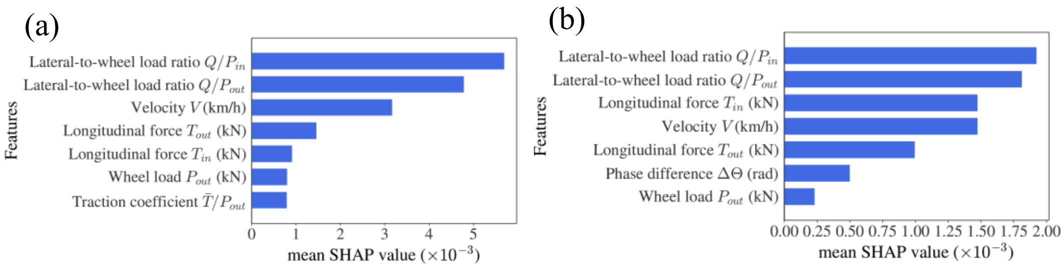


Figure 9: Mean SHAP value for the Friction Coefficient estimation model, where (a) and (b) represent the results of Pattern 1 and 2, respectively.

## 5 Conclusions

A machine learning–based method was proposed to estimate wheel–rail contact conditions from PQ measurement data, specifically the angle of attack, the contact position on the outer rail, and the friction coefficient. The estimation performance was evaluated by computing the RMSE between the ground truth and the estimated values through numerical simulations under conditions different from those used for training, including variations in vehicle load and the presence of track irregularities.
The results demonstrated that practical levels of accuracy were achieved across a wide range of vehicle speeds and curve radii, confirming the effectiveness of the proposed method.

## References


[1] S. Kuniyuki, T. Hondo, M. Suzuki, T. Miyamoto, and K. Nakano, “Estimation method of the motion state of a wheelset and the friction coefficient between wheel and rail using a single wheel creep force model for a railway vehicle

equipped with PQ wheelsets", Transactions of the JSME, 90(933). doi:10.1299/transjsme.23-00266, 2024, in Japanese.

[2] J.J. Kalker, "Three-Dimensional Elastic Bodies in Rolling Contact", Kluwer Academic Publishers, Dordrecht 1990.

[3] L. Xin, L. Xu, J. Zhang, M. Pei, J. Mao, and D. Wang, "Research on characterization methods for track irregularities", Railway Engineering Science, doi:10.1007/s40534-023-00325-1, 2024.

[4] A.R.B Berawi, "Improving Railway Track Maintenance Using Power Spectral Density (PSD)" PhD dissertation, University of Porto, 2013.

[5] G. Ke, Q. Meng, T. Finley, T. Wang, W. Chen, W. Ma, Q. Ye, and T.Y. Liu, "Lightgbm: A highly efficient gradient boosting decision tree", Advances in Neural Information Processing Systems (NIPS 2017), volume 30, 2017.

[6] S. Kiranyaz, O. Avci, O. Abdeljaber, T. Ince, M. Gabbouj, and D.J Inman, "1d convolutional neural networks and applications: A survey", Mechanical Systems and Signal Processing, 151, 107398, 2021.

[7] S. Kuniyuki, "Safety evaluation method for railway vehicles based on estimated contact conditions between wheel and rail", Doctor dissertation, The University of Tokyo, 2025 in Japanese.